Forward flight tests of a quadcopter UAV with various spherical body diameters

B. Theys*, J. De Schutter
Robotics Research Group, KU Leuven & Core Lab ROB, Flanders Make

ABSTRACT

This paper presents experimental results on the relation between forward airspeed, pitch angle and power consumption of a quadcopter UAV. The quadcopter consists out of an interchangeable spherical body, four cylindrical arms and small propellers mounted at $1m$ diagonal distance to minimize interference between body and propellers. This simple geometry facilitates results reproduction and comparison with simulation. Two different takeoff masses and four diameters of spherical bodies are tested for their steady-state speed and power for pitch angles up to $-45°$. The steady-state horizontal flight is recorded with on-board sensors at the end of flying long straight lines at a constant pitch angle in wind-still conditions. The best effective lift-to-drag ratio increases for smaller bodies and occurs at higher speeds for increasing mass. Results show that the equivalent frontal surface stays constant for pitch angles further than $-5°$ up to the maximum recorded $-45°$ and increases linearly with the frontal surface of the body.

1 INTRODUCTION

Multicopter UAVs, or 'drones', have become a popular platform for applications such as aerial imaging, mapping and inspection. These applications usually do not require high speeds or ranges but benefit of the vertical takeoff and landing (VTOL) capabilities of the multicopters. Moreover, in many countries, flying beyond visual line of sight (BVLOS) is not permitted yet. Therefore, most of today multicopter designs are optimized for maximum flight time and payload capacity near the hover flight condition. New applications in which the drones will fly BVLOS such as drone deliveries or offshore inspections, require long flight times, high speeds and range. The majority of published research on multicopters focuses on dynamics and control of the vehicles such as Huang [1] and Hoffmann [2] who incorporate the aerodynamics of multicopters by using helicopter theory to improve control when deviating significantly from the hover regime. Sufficient experimental data is required to develop models that can accurately predict the performance and can be used in improved control, design software or trajectory planning. However, there is only little published data for the flight performance of multicopters in forward flight. Schiano [3] performed wind tunnel experiments on a quadcopter to create data for a complete aerodynamic model. However, the experiments were carried out without turning propellers. Neumann et al. [4, 5] determined the relation between attitude and the wind velocity by performing wind tunnel experiments in hover and forward flight conditions to determine the 2D wind direction and speed when tracking hazardous gases. Russell [6] performed wind tunnel tests on five commercially available multicopters with varying geometries to determine forces, moments and power as function of the wind speed, rpm and attitude. Marino [7] performed wind tunnel tests to map the relation between power and the wind velocity vector to later use the multicopter as a flying wind sensor. Prudden [8] performed multiple experiments in wind tunnel conditions to map forward flight behavior. The focus was on the influence of frame geometry variations and the mutual interference between the rotors. For wind tunnel tests, creating a free-floating steady-state regime requires tuning the individual motor rpm to create a zero net force and moment. Next to that, vibrations created by the propulsion disturb these force readings or damage the sensor and for larger of heavier drones the propeller induced flow could significantly influence the wind tunnel flow. Rather than simulating steady-state flight conditions in a wind tunnel, this paper focuses on the forward flight regime with a constant speed and altitude in real outdoor flight in wind-still conditions as presented in figure 1.

Fig. 1: Multicopter with $0.5m$ spherical body in hover in wind-still conditions 10 $minutes$ before sunset.

*Email address: bart.theys@kuleuven.be

2 EXPERIMENT

2.1 *Components, configurations, conditions*

The geometry of the quadcopter consists out of an interchangeable sphere as body, four cylindrical arms with a diameter $20mm$ and a diagonal distance between the propeller shafts of $1m$. The Graupner 9x5 propellers for which the geometry is thoroughly described in [9], have a diameter of $0.23m$ which is small with respect to the distance between them to minimize the mutual interference and the interference with the body. Figure 2 illustrates these dimensions.

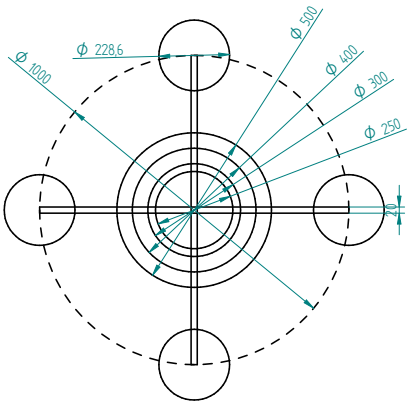

Fig. 2: quadcopter dimensions in mm with four different possible diameters of spherical body.

Figure 3 shows the multicopter fitted with a $40cm$ diameter spherical body during mass check right before takeoff.

Fig. 3: Multicopter fitted with a $40cm$ spherical *Styrofoam* body during mass check right before takeoff.

Table 1 lists an overview of the used components that complete the quadcopter test setup.

component	type	specifications
motor	T-motor 2216-11	900KV
ESC	FVT LittleBee30A	BLHeli Firmware
propeller	Graupner e-prop	9x5
voltage sensor	attopilot 45A	$15.70105\ V/V$
current sensor	attopilot 45A	$27.3224\ A/V$
flight controller	PixHawk	ArduCopter
battery	Zippy Li-Po 6s	$5000mah$, $30C$

Tab. 1: Used components for the test setup.

The four different diameters of hollow *Styrofoam* spheres can be fitted onto the body with cut-outs for the arms. Lead is added along the inner surface of the sphere to bring them all to the same mass. Table 2 presents an overview of the used spherical bodies.

diameter $[m]$	**foam mass** $[kg]$	**extra lead mass** $[kg]$
0.25	0.072	0.248
0.30	0.094	0.226
0.40	0.213	0.107
0.50	0.320	0

Tab. 2: *Styrofoam* spheres with different diameters used for the shape of the body, brought to a total mass of $0.320kg$.

With all bodies at the same mass, an additional lead mass can be added to achieve a total takeoff mass of $2.13kg$ and $2.50kg$ as presented in table 3.

component	**mass** $[kg]$
multicopter w/o bat. & body	1.00
battery	0.81
body	0.32
additional mass	0 - 0.37
total takeoff mass	2.13 - 2.50

Tab. 3: Mass distribution of the quadcopter for two different total masses.

Tests took place at two different days. Table 4 presents the atmospheric conditions at the time of the tests.

data set	**T** $[°C]$	**p** $[hPa]$	$V_{wind}[m/s]$	**humidity**
2.13 kg	23	1025	<1	65%
2.50 kg	28	1017	<1	45%

Tab. 4: Environmental conditions during the experiments. All experiments with the same mass are recorded consecutively without significant changes in conditions.

2.2 *Test procedure and data processing*

The goal of the test procedure is to record the power consumption and resulting speed in steady-state level flight of the quadcopter as a function of its pitch angle. Speed, endurance, range and payload capacity are fully determined if this relation is known for different total masses [7].

Flights are performed flying up and down one path at constant altitude. The pitch angle is gradually increased after each run up to a maximum pitch angle of $-45°$ and then decreased again for several consecutive runs up to $0°$. The results therefore contain measured cruise flight points in two flight directions so that any small wind speed would have minimum influence on overall accuracy of the result.

Figure 4 presents one run out of the recorded data during a flight. After turning the nose $180°$ with respect to the prior run, the multicopter is pitched $-45°$ and accelerates to a steady-state velocity of $20m/s$.

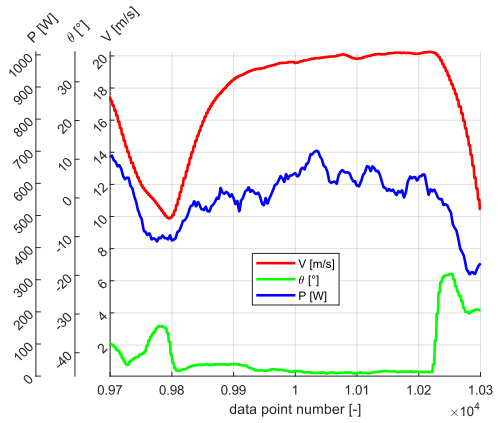

Fig. 4: Illustration of one run out of the recorded data during a flight. The multicopter accelerates to a steady-state velocity of $20m/s$ for a constant pitch angle of $-45°$.

Figure 5 presents the total power consumption and horizontal velocity as a function of the pitch angle for all recorded data during the test flight of the configuration with a total mass of $2.13kg$ and a $40cm$ body. The recorded data points during steady-state regimes at the end of each run are marked in orange. The top graph shows that even in steady-state the measured power fluctuates up to 25% around its mean value presented by the black dots. These variations are due to constant adjustments of the motor rpm for attitude and altitude control. The bottom graph shows there is also some variation of the resulting speed V for one run; there can be difference up to $2m/s$ between two runs with the same pitch angle. This can be explained by a wind speed of about $1m/s$ along the trajectory during the up and down run. Because both directions are flown, the accuracy of the overall experiment will not be influenced. For the further presentation of the results, the mean values for speed and power during the steady-state regimes are used.

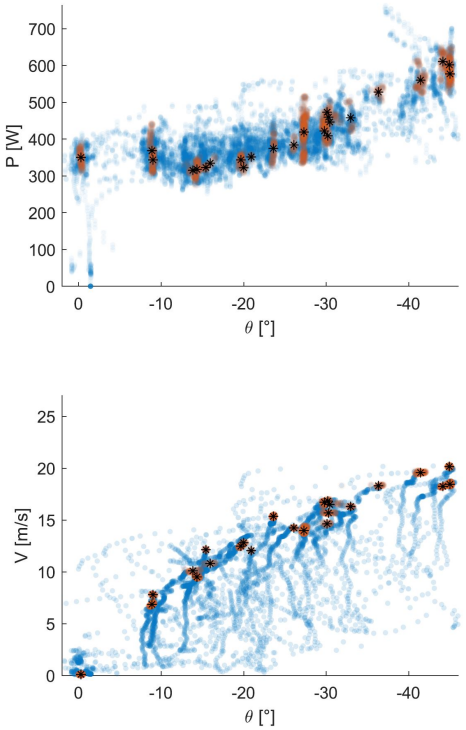

Fig. 5: Total power consumption and horizontal velocity as a function of the pitch angle for the configuration with $2.13kg$ and $40cm$. Blue: all recorded data during the test flight. Orange: recorded data during identified steady-state regime. Black: average values for each steady-state regime

This procedure is applied to all configurations resulting in eight data sets of steady-state horizontal flight power and speed as a function of the pitch angle that varies between $0°$ and $-45°$. Table 5 presents the number of steady-state horizontal flights that are identified per configuration and for which the results are presented in the next section.

	$25cm$	$30cm$	$40cm$	$50cm$
$2.13kg$	14	18	24	17
$2.50kg$	22	21	15	17
$2.93kg$	10	5	-	-

Tab. 5: Zones of steady-state horizontal flight recorded per configuration.

The initially planned total mass of $2.93kg$ was too heavy for the used propulsion for flying at high speeds, therefore only the hover data is used.

3 Results & Discussion

3.1 Resulting speed for increasing pitch angles

Figure 6 shows the cruise speed at pitch angles from hover to $-45°$ for the four different body diameters for the two total masses. Although the individual data points are not clearly separated, clear trends are visible. As expected, the resulting speed increases for decreasing body diameters and higher mass. For a higher total mass, the influence of the body diameter on the speed becomes larger and is more clear on the graph. For the $2.13kg$ experiments there is no noticeable difference in speed between the $25cm$ and $30cm$ sphere.

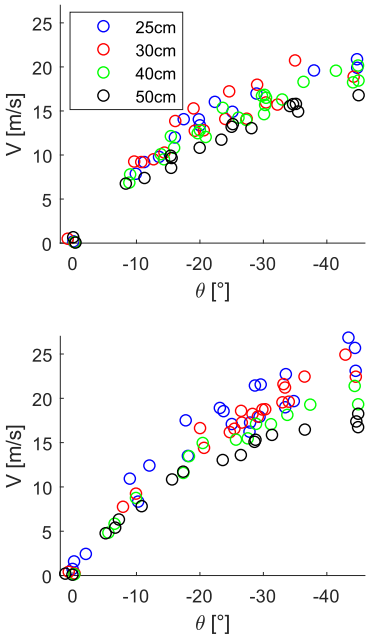

Fig. 6: Cruise speed at pitch angles from hover to $-45°$ for four different body diameters and two total masses. Top: 2.13kg. Bottom: 2.50kg.

To visualize the influence of body diameter and mass on the top speed, figure 7 shows the average top speed at $-45°$ pitch as a function of the body diameter for the two total masses. The top speed decreases for increasing body diameters and increases for a higher total mass. The difference in top speed for $2.13kg$ and $2.50kg$ of total mass is small for high body diameters and increases for decreasing body diameters. Although top speed for a given maximum pitch angle increases with mass, this is only possible if the propulsion system is capable of maintaining altitude at this high pitch angle and mass.

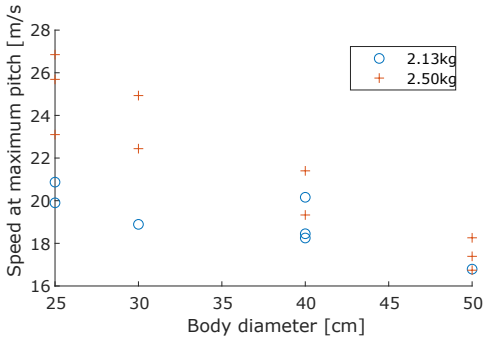

Fig. 7: Measured top speeds at $-45°$ as a function of the body diameter for two masses.

3.2 Power consumption in forward flight

Figure 8 shows the cruise power for pitch angles from hover to $-45°$ (left) or for speeds from hover to maximum speed (right) for four different body diameters and the two total masses. The required power slightly decreases at increasing speeds from hover which is in line with helicopter theory [10]. After reaching a minimum, the power increases significantly. The speeds at which minimum power is achieved lie higher for $2.50kg$ than for $2.13kg$ and the decrease of power with respect to hover is more pronounced for large body diameters.

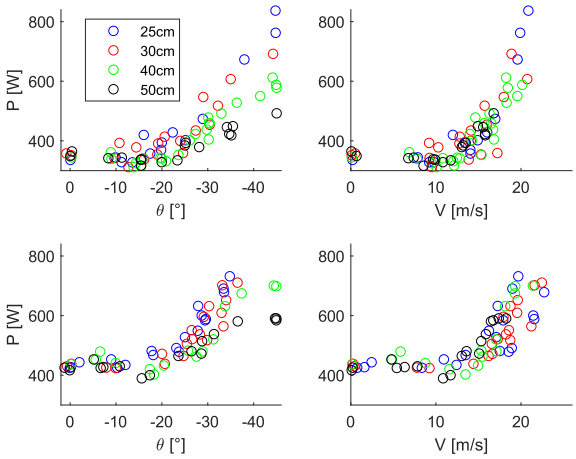

Fig. 8: Power as function of pitch θ and speed V for four different body diameters and two total masses. Top: $2.13kg$. Bottom: $2.50kg$.

3.3 Effective lift-to-drag ratio

The efficiency with which aircraft can move through the air can be expressed with the glide ratio, also known as the aerodynamic efficiency:

$$\frac{L}{D} = \frac{m_{tot}\, g}{D} = \frac{m_{tot}\, g\, V}{D\, V}[-], \tag{1}$$

in which $D\ V[W]$ presents the required power to fly. For a glider, this power can be directly calculated as the loss of potential energy. In other cases, an effective lift-to-drag ratio can be used, defined as:

$$\frac{eL}{D} = \eta_{prop}\ \frac{L}{D}\ = \frac{m_{tot}\ g\ V}{P}[-] \tag{2}$$

With P the required power from the energy source and η_{prop} the total efficiency of the propulsion system. For a multicopter this is the combined efficiency of the ESCs, motors and propellers.

Figure 9 shows the calculated effective lift-to-drag ratio between hover and the maximum speed at $-45°$ pitch for four different body diameters and two total masses. The maximum effective lift-to-drag ratios lie between 0.70 and 0.95. The speed at which the highest effective lift-to-drag ratio is achieved is higher for the experiments with $2.50kg$ compared to the experiments with $2.13kg$. The $2.50kg$ data set shows a trend of increasing maximum effective lift-to-drag ratios and the speeds at which they occur for decreasing body diameters. For the $2.13kg$ data set, this trend is less visible and between 12 to $13m/s$ the $40cm$ and $50cm$ bodies even seem to have a small advantage. This means the multicopter configurations with larger bodies consumed less power flying at this speed compared to the smaller diameters. This can be caused because less power is required from the propulsion system due to a decrease in drag, additional production of lift or an increase in efficiency of the propulsion system in this flight regime. Because spherical bodies of increasing diameter are used, the latter is the most likely explanation. As presented in figure 6 the pitch angle of the $25cm$ and $30cm$ body is approximately $-17°$ pitch for both and for the larger $40cm$ and $50cm$ body diameter approximately $-22°$ and $-25°$ pitch respectively which suggests that the propulsion system used in this paper is more efficient in these flight regimes.

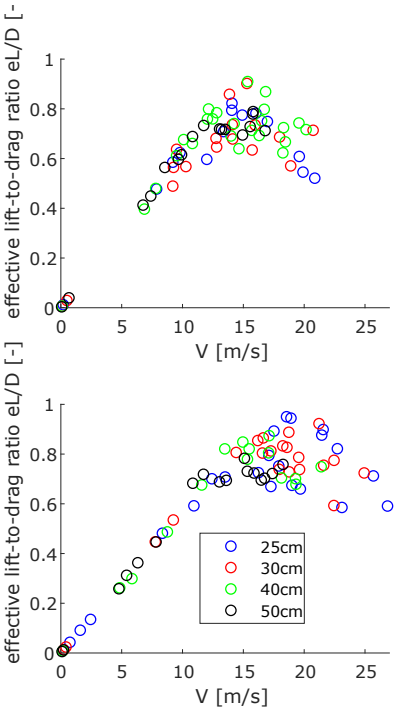

Fig. 9: Calculated effective lift-to-drag ratio at pitch angles from hover to $-45°$ for four different body diameters and two total masses. Top: $2.13kg$. Bottom: $2.50kg$.

3.4 Equivalent frontal surface

As it is common practice in helicopter performance identification [10], the drag of the body can be represented with an equivalent frontal surface area A_{eq} with $C_D = 1$:

$$D = \frac{1}{2}\ V^2\ \rho\ A_{front}\ C_D = \frac{1}{2}\ V^2\ \rho\ A_{eq}\ [N] \tag{3}$$

With V the speed and ρ the air density. For a multicopter without lifting surfaces and flying at a constant low speed, the forces that apply are the weight, drag and the force of the propellers. The latter one assumed to be along the shaft F_x. These forces are schematically presented in Figure 10.

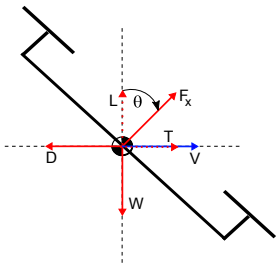

Fig. 10: Forces on a VTOL UAV without lifting surfaces at constant speed and altitude.

For this case, we can write the equivalent frontal surface as:

$$A_{eq} = \frac{2\ m_{tot}\ g\ \tan(-\theta)}{\rho\ V^2}\ [m^2] \tag{4}$$

Figure 11 shows the equivalent frontal surface at pitch angles from hover to $-45°$ for four different body diameters and two total masses. The equivalent frontal surfaces for data points between hover and $-5°$ pitch are not calculated because of the low value for speed in the denominator of equation 4. Although the data are scattered, different body diameters are clearly distinguishable in the data with a higher

body diameter resulting in a higher equivalent frontal surface. Between $-5°$ and $-15°$ the equivalent frontal surface shows a decreasing trend. Between $-15°$ and $-45°$ no clear trend is visible and the equivalent frontal surface could be approximated by a constant equal to the mean calculated value, presented by the horizontal lines.

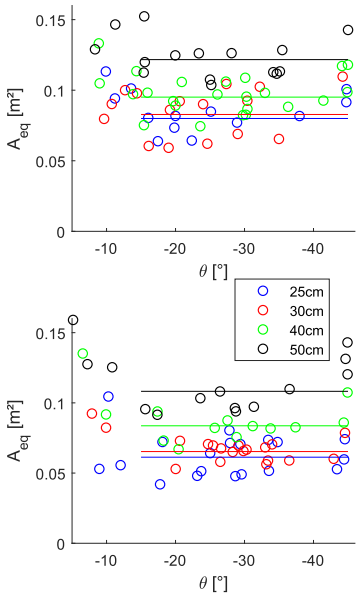

Fig. 11: Calculated equivalent frontal surface at pitch angles from hover to $-45°$ for four different body diameters and two total masses. The horizontal lines present the mean value for pitch angles from $-15°$ to $-45°$.

Figure 12 shows these mean equivalent frontal surface for angles between $-5°$ and $-45°$ as a function of the frontal surface of the spherical bodies for comparison.

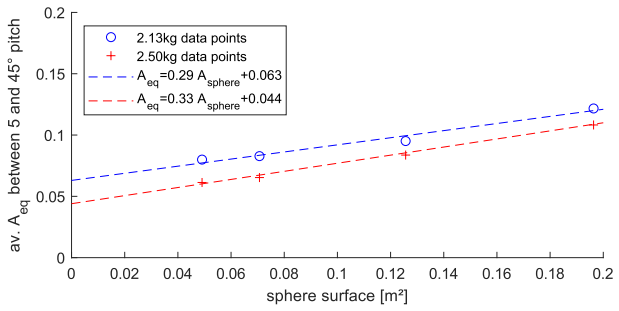

Fig. 12: Average calculated equivalent frontal surface for pitch angles between $-5°$ and $-45°$ for four different frontal surfaces of the spherical body and two total masses.

For the $2.13kg$ and $2.50kg$ data, a linear fit with slope 0.29 and 0.33 is found respectively. This lies within the expected drag coefficient of spherical bodies which, depending on the Reynolds number and surface quality lie between 0.1 and 0.5 [11]. Since the drag of the multicopter is not only due to the spherical body, there is an offset which takes into account the drag of the arms and motors with propellers. This offset is respectively $0.063m^2$ and $0.044m^2$ which would be the theoretical equivalent frontal surface of only the arms and propellers at -45 pitch.

3.5 Hover efficiency

As an example on how these data can be used for model validation, for the unique case of hover, the momentum theory as described by Rankine - Froude [12] and also known as the Actuator Disk Theory, can be used to predict the power as a function of the total mass m_{tot} and the total disk area covered by the propellers A_{disk}. The power required from the battery P_{batt} can be calculated with this basic model as:

$$P_{batt} = \frac{(m_{tot}\ g)^{1.5}}{\sqrt{2\ \rho\ A_{disk}}} \frac{1}{\eta_{esc}\ \eta_{mot}\ \eta_{plr}}\ [W] \tag{5}$$

With ρ the density of the air, g the gravity constant and $\eta_{esc}\ \eta_{mot}\ \eta_{plr}$ the efficiency of the ESC, motor and propeller respectively. The efficiency of the propeller is also referred to as the Figure of Merit [10].

Figure 13 shows the average of the measured hover power for three different masses. Next to $2.13kg$ and $2.50kg$ for the forward flight tests, a higher total mass of $2.93kg$ is tested in hover and added to this graph. A combined total efficiency η_{tot} of 44.3% for $\eta_{esc}\ \eta_{mot}\ \eta_{plr}$ resulted in a good fit.

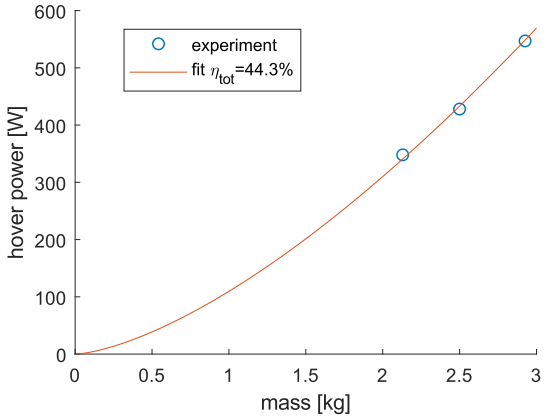

Fig. 13: Hover power and fit based on momentum theory with the assumption of a constant efficiency from battery power to kinetic energy of the accelerated air.

4 Conclusion and future work

Steady-state horizontal velocity and power of a quadcopter with a basic geometry and four interchangeable bodies of different diameters was tested at two total masses and pitch angles from $0°$ to $-45°$. Although experiments took place in wind-still conditions, there is significant variation in the measured data. However, clears trends were visible and the influence of different masses and shapes could be clearly identified. Results show that for a constant pitch angle, increased mass or smaller body diameter resulted in an increased speed. A maximum speed of approximately $27m/s$ was achieved for a $2.50kg$ total mass and $25cm$ body diameter at $-45°$ pitch. For every configuration, the minimum power did not occur during hover. A decrease in power is observed from hover to forward flight. The speed for minimum power increased for a higher mass. The difference between hover power and minimum power was more pronounced for increasing body diameters. The maximum effective lift-to-drag ratios for all configurations ranged between 0.70 and 0.95. The latter occurred at the heaviest configuration with the smallest body diameter. The equivalent frontal surface showed to be rather constant for each configuration for pitch angles between $-15°$ and $-45°$. With momentum theory clearly matching the results for hover, a total hover efficiency of 44.3% was found for the quadcopter in these experiments.

The data set obtained during the tests for this paper can be used as a reference for modeling the flight behavior of multicopter UAVs in forward flight. Trends are observed in the data but for further validation, more test data of different multicopters is required. Additional sensors can be added to monitor the individual states of each propulsion unit and measure rpm, voltage, current to allow also model validation of the propulsion system.

Acknowledgements

This research was funded by VLAIO grant HBC.2017.0198

References

[1] Haomiao Huang, Gabriel M. Hoffmann, Steven L. Waslander, and Claire J. Tomlin. Aerodynamics and control of autonomous quadrotor helicopters in aggressive maneuvering. *International Conference on Robotics and Automation*, 2009.

[2] Gabriel M Hoffmann, Haomiao Huang, Steven L. Waslander, and Claire J. Tomlin. Quadrotor helicopter flight dynamics and control: Theory and experiment. In *Proceedings of the AIAA Guidance, Navigation, and Control Conference*, volume 2, 2007.

[3] Schiano F. et al. Towards estimation and correction of wind effects on a quadrotor uav. *IMAV*, 2014.

[4] P. Neumann and M. Bartholmai. Real-time wind estimation on a micro unmanned aerial vehicle using its inertial measurement unit. *Sens. Actuators, A 235, 300310*, 2015.

[5] Neumann P. et al. Micro-drone for the characterization and self-optimizing search of hazardous gaseous substance sources: a new approach to determine wind speed and direction. *ROSE 2010-2010 IEEE International Workshop on Robotic and Sensors Environments, Proceedings, pp. 16*, 2010.

[6] Russel C. et al. Wind tunnel and hover performance test results for multicopter uas vehicles. *AHS 72nd Annual Forum*, 2016.

[7] Matthew Marino, Alex Fisher, Reece Clothier, Simon Watkins, Samuel Prudden, and Chung Sing Leung. An evaluation of multi-rotor unmanned aircraft as flying wind sensors. *International Journal of Micro Air Vehicles*, 7(3):285–299, 2015.

[8] Prudden S. et al. An investigation into the effects rotor wake interference on quadrotor uas forward flight performance. *18th Australian Aerospace Congress, Melbourne*, 2018.

[9] B. Theys, G. Dimitriadis, P. Hendrick, and J. De Schutter. Experimental and numerical study of mini-uav propeller performance in oblique flow. *AIAA Journal of Aircraft V.54-3 p1076-1084*, 2017.

[10] Raymond W. Prouty. *Helicopter performance, stability, and control*. 1995.

[11] S. F. Hoerner. *Fluid-Dynamic Drag*, page 455. 1965.

[12] W. Froude. On the elementary relation between pitch, slip, and propulsive efficiency. Technical Report 19930080719, National Advisory Committee for Aeronautics, Washington, DC, United States, 1920.